The onset of the Messinian salinity crisis in the deep Eastern Mediterranean basin

Published version:

DOI:10.1111/ter.12325

DR. VINICIO MANZI (Orcid ID : 0000-0002-6946-9750)

Article type : Paper

Received date: 21-Apr-2017
Revised version received date: 01-Dec-2017
Accepted date: 28-Dec-2017

Correspondence details:
Dr. Vinicio Manzi
Dipartimento di Scienze della Terra
Universita' degli Studi di Parma
Parma, PR 43124
Italy

Tel: 0521905354
E-mail: vinicio.manzi@unipr.it

THE ONSET OF THE MESSINIAN SALINITY CRISIS IN THE DEEP EASTERN MEDITERRANEAN BASIN

Vinicio Manzi,[*1,2], Rocco Gennari,[2,3.], Stefano Lugli,[4.], Davide Persico[1], Matteo Reghizzi[1], Marco Roveri,[1,2], B.C. Schreiber,[5], Rani Calvo,[6], Ittai Gavrieli,[6.], Zohar Gvirtzman,[6,7]

* corresponding author

[1] University of Parma, Parma, Italy

[2] ALP, Alpine Laboratory of Palaeomagnetism, Peveragno, CN, Italy

[3] University of Turin, Turin Italy

[4] University of Modena and Reggio Emilia, Modena, Italy

[5] University of Washington, Seattle, WA 98195, USA

[6] Geological Survey of Israel, Jerusalem, Israel

[7] Hebrew University, Jerusalem, Israel

ABSTRACT

Astronomical tuning of the Messinian pre-salt succession in the Levant Basin allows for the first time the reconstruction of a detailed chronology of the Messinian salinity

This article has been accepted for publication and undergone full peer review but has not been through the copyediting, typesetting, pagination and proofreading process, which may lead to differences between this version and the Version of Record. Please cite this article as doi: 10.1111/ter.12325

crisis (MSC) events in deep setting and their correlation with marginal records that supports the CIESM (2008) 3-stages model. Our main conclusions are:

i) MSC events were synchronous across marginal and deep basins;

i) MSC onset in deep basins occurred at 5.97 Ma;

ii) only foraminifera-barren, evaporite-free shales accumulated in deep settings between 5.97 and 5.60 Ma;

iii) deep evaporites (anhydrite and halite) deposition started later, at 5.60 Ma;

iv) new and published $^{87}Sr/^{86}Sr$ data, indicate that during all stages, evaporites precipitated from the same water-body in all the Mediterranean sub-basins;

The wide synchrony of events and $^{87}Sr/^{86}Sr$ homogeneity implies inter-sub-basin connection during the whole MSC and is not compatible with large sea-level fall and desiccation of the Mediterranean.

INTRODUCTION

Researches carried out on Mediterranean onshore successions that were originally deposited in shallow- (<200 m) and intermediate-water depth (200–1000 m) settings (Roveri et al., 2014a) showed that the Messinian salinity crisis (MSC; Hsü et al., 1973) onset occurred synchronously at 5.97 Ma (Manzi et al., 2013) and caused the sudden disappearance of the normal marine biota. For a long time, the MSC onset has been placed at the base of the evaporites, a criterion which is unsuitable, because evaporite precipitation occurred diachronously (CIESM, 2008; Manzi et al., 2007; 2016; Dela Pierre et al., 2011). In shallow-water settings primary gypsum is laterally replaced by carbonate or shale; in deeper, poorly oxygenated, settings only organic-rich shale and/or dolomitic limestone accumulated (Lugli et al., 2010). Thus, the onset of the MSC does not necessarily coincide with the onset of evaporite deposition (Roveri et al., 2014a; 2016).

The only places where primary evaporite deposition started at 5.97 Ma are those marginal shallow (<200 m) basins where the Primary Lower Gypsum (PLG; Lugli et al., 2010) unit accumulated during stage 1 (5.97–5.60 Ma). In intermediate depth basins (200–1000 m) organic-rich, foraminifera-barren shales were deposited during stage 1, whereas evaporites accumulated during stage 2 (5.60–5.55 Ma), forming a composite unit termed Resedimented Lower Gypsum (RLG), which includes gypsum, both primary cumulate and reworked PLG evaporites, and thick halite deposits (CIESM, 2008; Roveri et al., 2008; 2014a). During stage 2 the Mediterranean margins were deeply eroded forming the Messinian erosional surface (MES; Lofi et al., 2011), a key stratigraphic feature for shallow-to-deep correlations.

The deepest record of Messinian events is much less known as it is preserved in deep offshore areas and consequently it is only based on geophysical data. The timing and the origin of this deep record are still debated (Roveri et al., 2014a). In the Western Mediterranean, the deep evaporite unit is described with a typical threefold organization: a “flowing” salt body sandwiched between two bedded units (Hsü et al., 1973; Lofi et al., 2011; Roveri et al., 2014a). In the Levant basin the MSC deposits form a wedge-shaped unit (Bertoni and Cartwright, 2006; Gvirtzman et al., 2013; 2017) (Fig. 1) including mainly halite and subordinate terrigenous deposits (Feng et al., 2016) and showing: i) a gradual basinward thickening from few tens of meters at the eastern margin up to about 1800 m in the deeper portions (Gvirtzman et al., 2013); ii) a distinctive internal organization into 6 seismic sub-units (Gvirtzman et al., 2017); iii) an irregular erosional basal surface (“N reflector”; Hsü et al., 1973) associated with channelized features (Bertoni and Cartwright, 2006; Gvirtzman et al., 2013) which can be traced upslope into the canyons cut on the basin margin (Lugli et al., 2013); iv) a top truncation surface (“M reflector”; Hsü et al., 1973) possibly originated by the dilution of the Mediterranean water body at the end of stage 2 sealed by a thin (below seismic resolution) anhydrite unit (unit 7; Gvirtzman et al., 2017).

No stratigraphic constraints are available for these deep offshore Mediterranean successions, especially for their base. Consequently, onshore-offshore stratigraphic correlations remain highly speculative, thus hampering a full understanding of the MSC events.

RESULTS

The unique opportunity to analyze and to date a pre-MSC deep-water succession comes from the study of four industrial boreholes in the deep Levant basin (offshore Israel; Fig. 1) crossing the base of the Messinian salt unit. We carried out an integrated stratigraphic study based on well-logs, high-resolution seismic data, biostratigraphy (foraminifera and calcareous nannofossils), and geochemistry ($^{87}Sr/^{86}Sr$).

Biostratigraphy

We recognized six lower Messinian planktonic foraminifera bioevents in the fine-grained succession below the salt (Fig. 2, Tab. S1), which provide precise dating for well correlation. The total absence of foraminifera defines a “foraminifer barren interval” (FBI; Figs. 2 and 3) immediately below the evaporites. This interval corresponds to the Non-Distinctive Zone (NDZ) marking the MSC onset in onshore settings (Manzi et al., 2013; Iaccarino et al., 2007; Gennari et al., 2013; 2017). More detailed analyses were carried out on Aphrodite-2 borehole, where this interval is thicker.

This age definition is further confirmed by the distribution of calcareous nannofossil (Fig. 2; Fig. S1, Tab. S2). In Aphrodite-2 we recognized a prominent peak of *Sphenolitus abies* at 3961 m (Fig. S1), closely followed by a decrease of the number of species of calcareous nannofossil at 3958 m (Fig. 2; Fig. S1). Above this bioevent, up to 3937 m, the assemblage is oligotypic (Tab. S2), lacks open marine taxa and is dominated by r-selected opportunistic species (Wade and Bown, 2006). In other Mediterranean areas, like the Fanantello (Northern Apennines; Manzi et al., 2007), Pollenzo (Piedmont; Dela Pierre et al., 2011; Lozar et al., 2010) and Pissouri (Cyprus; Wade and Bown, 2006; Kouwenhoven et al., 2006) sections, the *S. abies* peak, which roughly coincides with the MSC onset, is also coupled with a similar stock of calcareous nannofossil taxa. The interval above 3937 m is barren except for two samples in the upper part of the salt unit, which contain rare marine nannofossils, including *Discoaster quinqueramus,* which went extinct at 5.54 Ma (Raffi et al., 2003) (Fig. 2; Fig. S1).

Moving from Aphrodite-2 toward the Israeli margin, the FBI is progressively eroded on top and the evaporites progressively cover older deposits (Fig. 2). Thus, the base of the evaporites, which is conformable in the Aphrodite-2, becomes unconformable toward the margin.

Well logs and cyclostratigraphy

Gamma ray (GR) and resistivity (RES) logs in the pre-evaporitic unit of Aphrodite-2 show a rhythmic alternation of “low GR–high RES” and “high GR–low RES” values (Fig. S3). This suggests a cyclical alternation of light marls and dark-grey shales, as confirmed by cuttings and drilling reports. A similar cyclical pattern, observed in coeval onshore basins in Spain (Sierro et al., 2001), Sicily (Hilgen and Krijgsman, 1999), Northern Apennines (Vai, 1997), Cyprus (Gennari et al., 2017) and in well-logs of the Balearic offshore (Ochoa et al., 2015), is usually interpreted as related to precession-driven climatic oscillations (Hilgen and Krijgsman, 1999).

Between the depth of 3996 m and the evaporites base, we found 33 cycles, which is the expected number of precessional cycles between bioevents 3 and 11, roughly corresponding to a 700-ka interval. Moreover, the GR log shows 8 intervals with a smaller variability (marked by arrows in Fig. 2) separating longer (4-5 cycles) intervals with larger GR variability. This pattern is commonly considered as the result of the eccentricity (red curve in Fig. 2) interference on the precession signal (Ochoa et al., 2015; Sierro et al., 2000). The low GR variability intervals match the expected position of eccentricity minima based on our biostratigraphic results, supporting an astronomical origin of the lithological cyclicity inferred from the GR-RES log. Consequently, we anchored the interval with low GR variability with the 8 eccentricity minima and tuned the GR curve with the insolation curve; in this way, we were able to define a high-resolution age calibration of the succession below the salt. The calculated sedimentation rate of ~90 mm/ka is in good agreement with those of other pre-MSC peri-Mediterranean successions (Fig. S2). The highest occurrence (HO) of foraminifera, 6 m above the HO of *T. multiloba*, corresponds to the em5 eccentricity minimum and marks the MSC onset in the onshore successions (Manzi et al., 2013) at 5.971 Ma.

Spectral analysis

In order to support our cyclostratigraphic interpretation, we performed a spectral analysis on the age-constrained pre-MSC GR record of Aphrodite-2 borehole (3997–3958 m depth interval) and found a dominant frequency peak of 2.46 m (Fig. 4b) corresponding to ~28 ka; this is partially overlapped by two less prominent peaks at 3.2 and 1.89 m corresponding to ~36 and 21 ka respectively.

The cross spectral analysis of GR and insolation (Fig. 4c) shows high coherence peaks (over 95% and around 90%) linked to precession, at 19.3 ka and 24.8 ka. Obliquity is expressed by a single peak, at 43.1 ka, showing a coherence lower than precession. These results suggest a good control of the precession component with a minor control of the obliquity signal. The 27 m-thick foraminifera-barren interval just below the evaporites contains 16 GR-based lithological cycles. Assuming a precessional origin for these cycles, a duration of ~350 ka can be estimated for the FBI.

^{87}Sr/^{86}Sr isotopic *analysis*

In Aphrodite-2, the FBI is overlain by a thin (5.5 m) anhydrite/shale unit (unit 0) and, in turn, by very thick (up to 1800 m) salt body separable into 6 seismic sub-units, which are tilted basinward and truncated landward and covered by a thin anhydrite-rich unit (unit 7) (Figs. 5 and 6; Gvirtzman et al., 2013; 2017). The salt body in Aphrodite-2 and Hannah-1 boreholes (Fig. 5, Tab. S3; Fig. S4) shows some ^{87}Sr/^{86}Sr values higher than the global ocean field, but is mainly characterized by values typical of stages 1 and 2 (e.g. 0.7088–0.70906; Roveri et al., 2014b; Gvirtzman et al., 2017); values < 0.7088, which are typical of stage 3, were not found.

DISCUSSION

The data from Aphrodite-2 indicate that the FBI found below the evaporites could record the whole MSC stage 1 and that no significant hiatus is present below the evaporites in this area. Moving eastward toward the Israeli margin the base of the evaporites becomes progressively erosive and can be traced within the Ashdod canyon, where clastic evaporites have been found (Lugli et al., 2013). It follows that the base of the evaporites can be identified as the Messinian erosional surface (MES) in the margins and by its correlative conformity (MES-cc) in the deep part of the basin. This situation is similar to what documented in the Northern Apennines (Manzi et al., 2007) where a 60 m-thick organic-rich barren shale unit, that has been identified as the deep-water counterpart of the PLG (Manzi et al., 2007; Lugli et al., 2010) of stage 1, is overlain by a unit made of clastic evaporites (Manzi et al., 2005), derived from dismantling and resedimentation of the PLG during stage 2. Such units are usually found above fine-grained organic-rich foraminifera-barren deposits in relatively deep settings, where PLG did not accumulate (Manzi et al., 2007; 2011; Roveri et al., 2016); in Sicily, Calabria and Cyprus these deposits are associated with halite (CIESM, 2008; Roveri et al., 2008; 2014a; Manzi et al., 2016).

The Sr isotope stratigraphic significance for the salinity crisis interval has been assessed in various papers for sulfates and carbonates (Müller and Mueller, 1991; Flecker et al., 2002; Roveri et al., 2014a and references therein). The Sr isotope composition presented here for halite are in the range of stage 1 and 2, but show some anomalous values higher than the global ocean curve (Fig. 6). Compared to sulfates, halite may incorporate an extremely lower proportion of Sr and may show a depositional rate up to one order of magnitude higher. It follows that halite isotope composition may be very sensitive for local diverse, short term Sr input (see supplementary material). Despite the anomalous values, the deposition of the halite body during stage 1 or 2 is supported by the range of values obtained for the sulfates found in the salt body, which are within the field of stage 1 or 2 (Fig. 6; Tab. S5).

The recognition below the salt in Aphrodite-2 of the FBI which is recording the entire stage 1, implies that the main halite body (Units 1-6) was not precipitated during stage 1.

On the other hand, the clastic-rich evaporites of Unit 7, which is capping the salt body, yielded Sr isotope values typical of stage 3 (Or-South-1 borehole, Gvirtzman et al., in 2017) and is overlain in the Israeli margin by an evaporite-free unit containing Lagomare fossil assemblages (Derin, 2000).

The inescapable conclusion is that the salt unit, being sandwiched between the FBI (stage 1) and Unit 7 (stage 3), must have been accumulated during stage 2. This interpretation is also supported by the recovery of *Discoaster quinqueramus* (Fig. S1; Tab. S2) within unit 5 of the halite complex, which went extinct towards the end of stage 2.

Further considerations on the duration of halite deposition in the Levan Basin can be deduced from seismic facies and well logs, both showing alternation from nearly pure halite units (seismically transparent) to well bedded units (reflection-rich) containing thin layers of clays (Gvirtzman et al., 2013; Feng et al., 2016, Fig. S4). According to Roveri et al. (2014b) and Manzi et al. (2016), we suggest that these seismic facies may reflect precessional-controlled alternations of relatively arid/humid climate marked by low/high terrigenous supplies.

The $^{87}Sr/^{86}Sr$ data suggest that Levant basin was not isolated from the Global Ocean (McArthur et al., 2012) before, during or after the deposition of the main halite unit (Gvirtzman et al., 2017); thus, implying the persistence of the Mediterranean Sea level at a relatively high-stand conditions (at least higher than intra-basinal sills) in order to allow the Atlantic inflow to reach the Eastern Mediterranean.

It follows that our data do not support the hypothesis of a complete desiccation of the Mediterranean Sea during the salinity crisis (Hsü et al., 1973).

CONCLUSIONS

The MSC succession in the deep Eastern Mediterranean are characterized by the following features:

- the crisis onset started synchronously at 5.97 Ma; it is marked by the disappearance of foraminifera and the peak of *S. abies*;
- the stage 1 is recorded by an evaporite-free unit barren in foraminifers (FBI) and containing only opportunistic calcareous nannofossil taxa with a decreasing-upward trend of abundance;
- the thickness of FBI is limited and below seismic resolution;
- the FBI is progressively truncated at its top by an erosional surface at the base of the evaporites moving eastward from the deep part of the basin toward the Israeli margin; this surface can be traced upslope into the canyons of the Israeli margin, where clastic evaporites deriving from the dismantlement of the PLG unit (Lugli et al., 2013) were deposited; we interpret this surface as the Messinian erosional surface (MES) passing downslope to its correlative conformity surface (MES-cc);
- the deposition of the main salt unit started only at 5.60 Ma, during stage 2;
- $^{87}Sr/^{86}Sr$ data show that halite precipitated from a water body still connected with the global Ocean.

Our findings indicate that the Messinian successions share the same timing and arrangement in both marginal and deep settings and resemble the successions deposited elsewhere in intermediate-depth onshore marginal basins (Roveri et al., 2014a; 2016). This suggests that all the Mediterranean sub-basins, regardless of their water depth, remained hydrologically connected also during the acme of the crisis. An obvious implication is that the usually envisaged high-amplitude sea level oscillations and the desiccation of the Mediterranean Sea are not supported by these data, thus suggesting that alternative scenarios of the MSC are possible (Roveri et al., 2014c; 2016).

ACKNOWLEDGMENTS

We acknowledge Modiin Energy and Pelagic partnership for their permission to release seismic and well data. UNIPR and UNIMORE research funds covered costs of Sr analyses. We thank A. Cipriani for facilitating these analyses at the UNIMORE laboratory. Journal Editor (M. Coleman), Associate Editor, and three reviewers (N. Mitchell, J. Lofi, and Y. Druckman) are greatly acknowledged for their suggestions that led us to improve the earlier version of the manuscript.

REFERENCES

Bertoni, C., Cartwright, J.A., 2006. Controls on the basinwide architecture of Messinian evaporites on the Levant margin (Eastern Mediterranean). Sedimentary Geology, 188–189, 93–114.

CIESM, 2008. The Messinian salinity crisis from mega-deposits to microbiology. In: Briand, F. (Ed.), A consensus report, in 33ème CIESM Workshop Monographs, 33. CIESM, 16, bd de Suisse, MC-98000, Monaco, pp. 1–168

Dela Pierre, F., Bernardi, E., Cavagna, S., Clari, P., Gennari, R., Irace, A., Lozar, F., Lugli, S., Manzi, V., Natalicchio, M., Roveri, M., Violanti, D., 2011. The record of the Messinian salinity crisis in the Tertiary Piedmont Basin (NW Italy): the Alba section revisited. Palaeogeography, Palaeoclimatology, Palaeoecology, 310, 238–255.

Derin, B., 2000, Stratigraphic and environments of deposition of Or South 1075–2090 m: Ramat Gan, Israel, Drerin Consulting & Micropaleontologi- cal Services LTD, Internal Isramco Consultant Report 2/00, 10 p.

Flecker, R., S. de Villiers, and R. M. Ellam (2002), Modelling the effect of evaporation on the salinity - 87Sr/86Sr relationship in modern and ancient marginal - marine systems: the Mediterranean Me ssinian Salinity Crisis, Earth Planet. Science Letters, 203, 221-233.

Feng, Y.E., Ynkelzon, A., Steingberg J., Reshef M., 2016. Lithology and characteristics of the Messinian evaporite sequence of the deep Levant Basin, eastern Mediterranean Marine Geology, 376, 118–131.

Gennari R., Lozar F., Turco E., Dela Pierre F., Lugli S., Manzi V., Natalicchio M. Roveri M., Schreiber B.C., Taviani M., 2017. Integrated stratigraphy and paleoceanographic evolution of the pre-evaporitic phase of the Messinian salinity crisis in the Eastern Mediterranean as recorded in the Tokhni section (Cyprus Island). Newsletters on Stratigraphy. DOI:10.1127/nos/2017/0350

Gennari, R., Manzi, V., Angeletti, L., Bertini, A., Biffi, U., Ceregato, A., Faranda, C., Gliozzi, E., Lugli, S., Menichetti, E., Rosso, A., Roveri, M., Taviani, M., 2013. A shallowwater record of the onset of theMessinian salinity crisis in the Adriatic foredeep (Legnagnone section, Northern Apennines). Palaeogeography, Palaeoclimatology, Palaeoecology, 386, 145–164.

Gvirtzman, Z., Reshef, M., Buch-Leviatan, O., Ben-Avraham, B., 2013. Intense salt deformation in the Levant Basin in themiddle of the Messinian Salinity Crisis. Earth and Planetary Science Letters, 379, 108–119.

Gvirtzman Z., Manzi V., Calvo R., Gavireli I., Gennari R., Lugli S., Reghizzi M., Roveri M., 2017. Intra-Messinian truncation surface in the Levant Basin explained by subaqueous dissolution. Geology, 45 (10), 915-918.

Hilgen, F.J., Krijgsman, W., 1999. Cyclostratigraphy and astrochronology of the Tripoli diatomite formation (pre-evaporite Messinian, Sicily, Italy). Terra Nova, 11, 16–22.

Hsü, K., Ryan, W.B.F., Cita, M., 1973. Late Miocene desiccation of the Mediterranean. Nature, 242, 240.

Iaccarino, S.M., Premoli Silva, I., Biolzi, M., Foresi, L.M., Lirer, F., Turco, E., Petrizzo, M.R., 2007. Practical manual of Neogene Planktonic foraminifera. International School on Planktonic Foraminifera. VI course: Neogene. Perugia.

Kouwenhoven, T.J., Morigi, C., Negri, A., Giunta, S., Krijgsman, W., Rouchy, J.M., 2006. Palaeoenvironmental evolution of the eastern Mediterranean during the

Messinian: constraints from integrated microfossil data of the Pissouri Basin (Cyprus). Marine Micropalaeontology, 60, 17–44.

Laskar, J., Fienga, A., Gastineau, M., Manche, H., 2011. La2010: A new orbital solution for the long-term motion of the Earth. Astron. Astrophys., Volume 532, A89

Lofi, J., Déverchère, J., Gaullier, V., Gillet, H., Gorini, C., Guennoc, P., Loncke, L., Maillard, A., Sage, F., Thinon, I., 2011. Seismic atlas of the "Messinian Salinity Crisis" markers in the Mediterranean and Black seas. Commission for the Geological Map of the World and Memoires de la Société Géologique de France, Nouvelle Série, p. 72.

Lozar, F., Violanti, D., Dela Pierre, F., Bernardi, E., Cavagna, S., Clari, P., Irace, A., Martinetto, E., Trenkwalder, S., 2010. Calcareous nannofossils and foraminifers herald the Messinian salinity crisis: the Pollenzo section (Alba, Cuneo; NW Italy). Geobios 43, 21–32.

Lugli, S., Gennari, R., Gvirtzman, Z., Manzi, V., Roveri, M., Schreiber, B.C., 2013. Evidence of clastic evaporites in the canyons of the Levant Basin (Israel): implications for the Messinian Salinity Crisis. Journal of Sedimentary Research, 83, 942–954.

Lugli, S., Manzi, V., Roveri, M., Schreiber, B.C., 2010. The Primary Lower Gypsum in the Mediterranean: a newfacies interpretation for the first stage of theMessinian salinity crisis. Palaeogeography, Palaeoclimatology, Palaeoecology, 297, 83–99.

Manzi V., Lugli S., Roveri M., Dela Pierre F., Gennari R. Lozar F., Natalicchio M., Schreiber B.C., Taviani M., Turco E., 2016. The Messinian salinity crisis in Cyprus: a further step towards a new stratigraphic framework for Eastern Mediterranean. Basin Research, 28, 207-236.

Manzi, V., Gennari, R., Hilgen, F., Krijgsman, W., Lugli, S., Roveri, M., Sierro, F.J., 2013. Age refinement of theMessinian salinity crisis onset in the Mediterranean. Terra Nova, 25, 315-322.

Manzi, V., Lugli, S., Ricci Lucchi, F., Roveri, M., 2005. Deep-water clastic evaporites deposition in the Messinian Adriatic foredeep (northern Apennines, Italy): did the Mediterranean ever dry out? Sedimentology, 52, 875-902.

Manzi, V., Lugli, S., Roveri, M., Schreiber, B.C., Gennari, R., 2011. The Messinian "Calcare di Base" (Sicily, Italy) revisited. Geological Society of America Bulletin 123, 347-370.

Manzi, V., Roveri, M., Gennari, R., Bertini, A., Biffi, U., Giunta, S., Iaccarino, S.M., Lanci, L., Lugli, S., Negri, A., Riva, A., Rossi, M.E., Taviani, M., 2007. The deep-water counterpart of the Messinian Lower Evaporites in the Apennine foredeep: the Fanantello section (Northern Apennines, Italy). Palaeogeography, Palaeoclimatology, Palaeoecology, 251, 470-499.

McArthur, J.M., Howarth, R.J., Shields, G.A., 2012. Strontium Isotope Stratigraphy. In: Gradstein, F.M., Ogg, J.G., Schmitz, M., Ogg, G., 2012. The Geologic Time Scale. Elsevier.

Müller, D.W., Mueller, P.A., 1991. Origin and age of the Mediterranean Messinian evaporites: implications from Sr isotopes. Earth Planetary Science Letters, 107, 1–12.

Ochoa D., Sierro F.J., Lofi J., Maillard A., Flores J.-A., Suarez M., 2015. Synchronous onset of the Messinian evaporite precipitation: First Mediterranean offshore evidence. Earth and Planetary Science Letters, 427, 112-124.

Raffi, I., Mozzato, C.A., Fornaciari, E., Hilgen, F.J., Rio, D., 2003. Late Miocene calcareous nannofossil biostratigraphy and astrobiochronology for the Mediterranean region. Micropaleontology, 49, 1–26.

Roveri, M., Lugli, S., Manzi, V., Schreiber, B.C., 2008. The Messinian Sicilian stratigraphy revisited: toward a new scenario for the Messinian salinity crisis. Terra Nova 20, 483–488.

Roveri M., Gennari. R, Lugli S., Manzi V., Minelli N., Reghizzi M., Riva A., Rossi M.E., Schreiber B.C., 2016. The Messinian salinity crisis: open problems and possible implications for Mediterranean petroleum systems. Petroleum Geoscience, 22, 283-290.

Roveri M., Lugli S., Manzi V., Gennari R., and Schreiber B.C., 2014b. High-resolution strontium isotope stratigraphy of the Messinian deep Mediterranean basins: implications for marginal to central basins correlation. Marine Geology, 349, 113-125.

Roveri, M., Flecker, R., Krijgsman, W., Lofi, J., Lugli, S., Manzi, V., Sierro, F.J., Bertini, A., Camerlenghi, A., De Lange, G.J., Govers, R., Hilgen, F.J., Hubscher, C., Meijer, P.T., Stoica, M., 2014a. The Messinian Salinity Crisis: past and future of a great challenge for marine sciences. Marine Geology, 349, 113–125.

Roveri, M., Manzi, V., Bergamasco, A., Falcieri, F., Gennari, R., Lugli, S., 2014c. Dense shelf water cascading and Messinian canyons: a new scenario for the Mediterranean salinity crisis. American Journal of Science, 314, 751–784.

Sierro, F.J., Hilgen, F.J., Krijgsman, W., Flores, J.A., 2001. The Abad composite (SE Spain): a Messinian reference section for the Mediterranean and the APTS. Palaeogeography, Palaeoclimatology, Palaeoecology, 168, 141–169.

Sierro, F.J., Ledesma, S., Flores, J.A., Torrescusa, S., Martinez del Olmo, W., 2000. Sonic and gamma-ray astrochronology: Cycle to cycle calibration of Atlantic climatic records to Mediterranean sapropels and astronomical oscillations. Geology, 28, 8, 695-698.

Vai, G.B., 1997. Cyclostratigraphic estimate of the Messinian Stage duration. In: Montanari, A., Odin, G.S., Coccioni, R. (Eds.), Miocene Stratigraphy: An Integrated Approach. Developments in Paleontology and Stratigraphy, 15, pp. 463–476.

Van der Laan, E., Hilgen, F.J., Lourens, L.J., de Kaenel, E., Gaboardi, S., Iaccarino, S., 2012. Astronomical forcing of Northwest African climate and glacial history during the late Messinian (6.5–5.5 Ma) Palaeogeography, Palaeoclimatology, Palaeoecology, 313-314, 107-126.

Wade, B.S., Bown, P., 2006. Calcareous nannofossils in extreme environments: the Messinian Salinity Crisis, Polemi Basin, Cyprus. Palaeogeography, Palaeoclimatology, Palaeoecology, 233, 271–286.

Supplementary material:

FV_supplementary: Description of the different methodologies adopted for this work.

Supplementary figures captions:

FIG. S1. Aphrodite-2 borehole calcareous nannofossils distribution. The recognized bioevents are: 9 - AP of S. abies; 11 - HCO normal marine calcareous nannofossils; 14 - HO calcareous nannofossils; MCNI: marine calcareous nannoplankton influx, containing rare *Discoaster quinqueramus* whose HO is placed at 5.54 Ma (Raffi et al., 2003).

FIG. S2. Estimated sedimentation rate of the Aphrodite-2 borehole pre-evaporitic successions and comparison with other reference sections. Atlantic: Ain El Beida (Van der Laan et al., 2006); Loulja (Van der Laan et al., 2006). Western Mediterranean: Perales (Sierro et al., 2001); Muchamiel (Ochoa et al., 2015). Northern Mediterranean: Fanantello (Manzi et al., 2007), Monte del Casino (Manzi et al., 2013); Trave (Iaccarino et al., 2008); Eastern Mediterranean: Gavdos (Krjigsman et al., 2004); Tokhni (Gennari et al., in press); Pissouri (Krijgsman et al., 2002); Levant basin Miocene average (Feng et al., 2016); Southern Mediterranean: Zakynthos (Karakitsios et al., 2016); Falconara (Hilgen and Krijgsman, 1999; Blanc-Valleron et al., 2002).

FIG. S3. Well logs of the succession encompassing the base of the evaporites registered in the Aphrodite-2, Myra-1 and Sara-1 boreholes and their lithological interpretations base also on cutting analyses.

FIG. S4. Gamma Ray and Resistivity logs of the Aphrodite-2 borehole and the correspondence with the seismic units defined by Gvirtzman et al. (2017). The alternation of halite units with higher or minor terrigenous content has tentatively correlated with humid or arid periods.

Supplementary Tables Captions

TAB. S1. Bio and magnetostratigraphic events for the MSC.

TAB. S2. Aprodite-2 borehole calcareous nannofossils range chart.

TAB. S3. Myra-1 borehole calcareous nannofossils range chart.

TAB. S4. Sara- borehole calcareous nannofossils range chart.

TAB. S5. Results of the Strontium isotopes analyses.

FIGURE CAPTIONS

FIG.1. A) location of the study area. B) structural map of the base of the MSC evaporites (N reflector) with location of the studied boreholes; Ashdod-2 borehole data are from Lugli et al. (2013). Black boxes indicate seismic images of figure 1C). trace of section in C and in figure 4 is reported. C) seismic-based cross section of the Levant basin. Notice the wedge-shaped main halite unit lying between the M and the N seismic reflectors. Because of the insufficient seismic resolution, N reflector includes the FBI and unit 0M reflector include unit7.

FIG.2. Stratigraphic correlation among the studied boreholes and the main reference sections of the Mediterranen, in shallow (Monte Tondo and Monticino composite section; Manzi et al., 2013) and in intermediate-depth settings (Fanantello; Manzi et al., 2007; black debris concentration used for tuning is also reported), and of the Atlantic (Ain El Beida; Van der Laan et al., 2012). The δ^{18}O curve from Ain El Beida (Van der Laan et al., 2012) is also shown. Notice the good correspondence between the gamma ray (GR) of the pre-evaporitic unit of Aphrodite and the insolation curve (Laskar et al., 2011). Earth eccentricity minima (em1 to em8) used for tuning are also shown. The foraminifera-barren interval (FBI; light purple area) is the evaporite-free unit representing the deep time-equivalent of stage 1 evaporites (Primary Lower Gypsum; PLG). The foraminifer bioevents allowed the attribution of the pre-evaporitic successions to the Messinian zones12 MMi13b - MMi3c (pars) in Sara1 and MMi13b (pars), MMi13c and NDZ (Non Distinctive Zone10) in Aphrodite2. (see. Tab. S1 for age references). **Bio-magneto stratigraphic events:** 1) HO *G. nicolae* (6.710 Ma); 2) LO *N. amplificus* (6.684 Ma); 3) HO *G. miotumida* (6.500 Ma); 4) LO *T. multiloba* (6.410 Ma); 5) L/R *N. acostaensis* coling change (6.340 Ma) = MMi3c base; 6) AB *T. multiloba* (6.210 Ma); 7) AE *T. multiloba* (6.040 Ma); 8) base of Gilbert chron (6.035 Ma); 9) AP of *S. abies* (5.974 Ma); 10) HO foraminifera (5.971 Ma) = base of Non Distinctive Zone; 11) HCO normal marine calcareous nannofossils (5.970 Ma); 12) sharp decrease in abundance and diversity of calcareous nannofossils (5.970 Ma);

13) HO *N. amplificus* (5.939 Ma); 14) HO calcareous nannofossils (5.750-5.640 Ma); 15) HO *D. quinqueramus* (5.540 Ma).

FIG.3. Planktonic foraminifers distribution in Aphrodite-2, Myra-1 and Sara-1 boreholes. The recognized bioevents are: 5 - L/R *N. acostaensis* coling change (6.340 Ma); 6 - AB *T. multiloba* (6.210 Ma); 7 - AE *T. multiloba* (6.040 Ma); 10 - HO foraminifera (5.971 Ma) and base of Non Distinctive Zone (Iaccarino et al., 2007). FBI, Foraminifer barren interval.

FIG.4. Spectral analyses on the gamma ray (GR) record of the Aphrodite 2 borehole. A) Age model and time constraints used for the tuning of the gamma ray curve. B) Power spectrum and evolutive spectrum of the GR in depth domain. Notice the good persistence of the peak with a period of 2.46 m. C) Results of spectral analysis: in the upper part the power spectra for GR (pink) and insolation 65° N (gray) for the investigated time window; in the lower part the coherence calculated after the spectral analysis. Non-zero coherence is higher than: 0.38413 (80%); 0.477452 (90%); 0.550595 (95%). The precession-related periodicities (19 and 23 Kyr) have a very high coherence, whereas the obliquity-related ones have a slightly lower coherence.

FIG.5. Schematic seismic section (a) of the Levant basin showing the stratigraphic position of the samples and the results of the Sr isotopic analyses (b) of this work (TW) compared with other published data of the Levant basin (L13, Lugli et al., 2013; G17, Gvirtzman et al., 2017). The main salt unit show a signature typical of the stage 1+2 of the MSC and are in agreement with those obtained from the clastic evaporite onshore (Ashdod-2; Lugli et al., 2013). This, suggests that the halite precipitated from a water body connected with the Western Mediterranean and with the global ocean. It is worth noting that Sr values obtained from unit 0 to unit 5 are markedly different from those obtained from the stage 3 evaporites of unit 7 (Gvirtzman et al., 2017).

FIG.6. Sr isotope data from the Levant basin (this work) compared to the other Mediterranean areas (Roveri et al., 2014) implemented with published data from the Levant basin (L13, Lugli et al., 2013; G17, Gvirtzman et al., 2017).

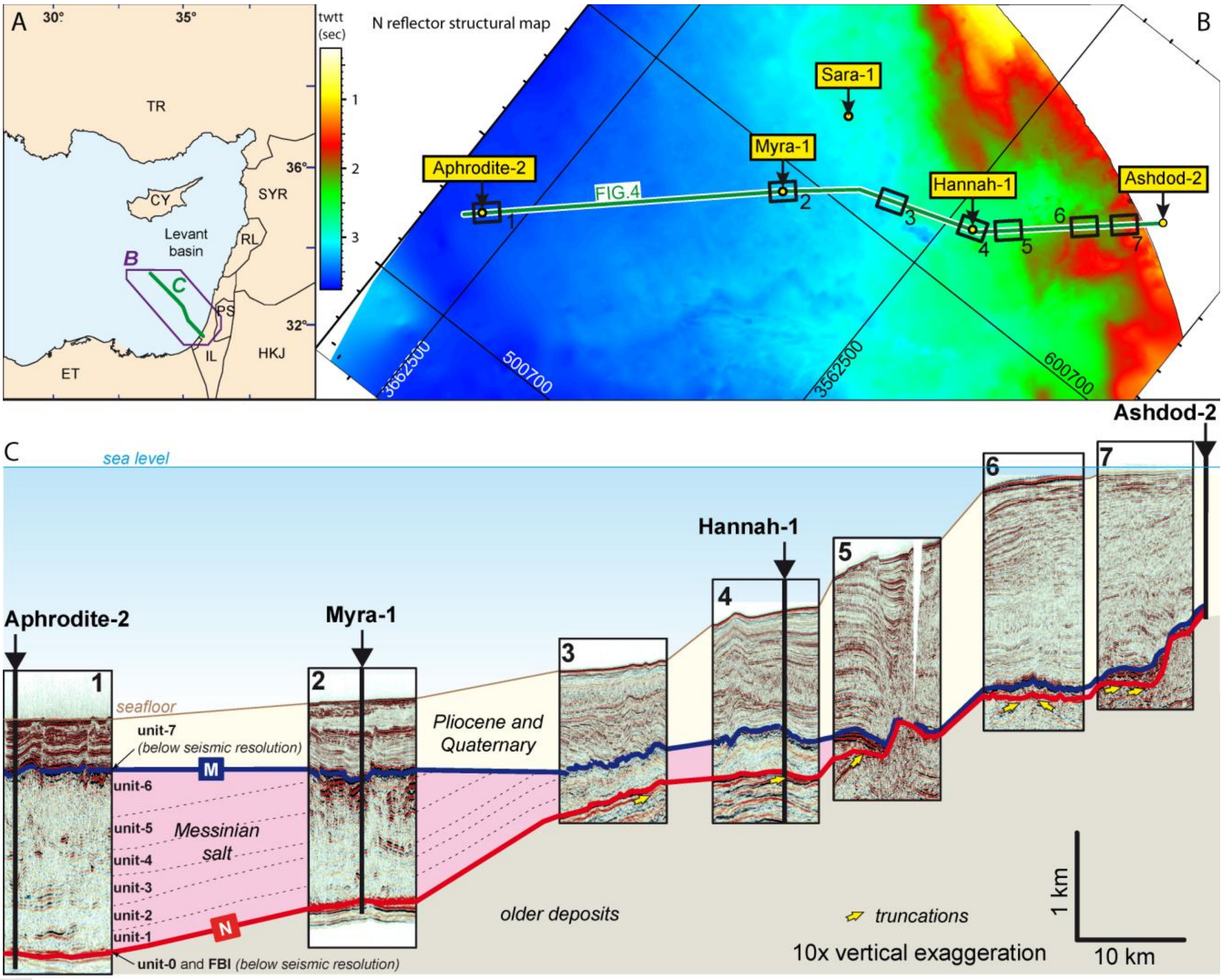

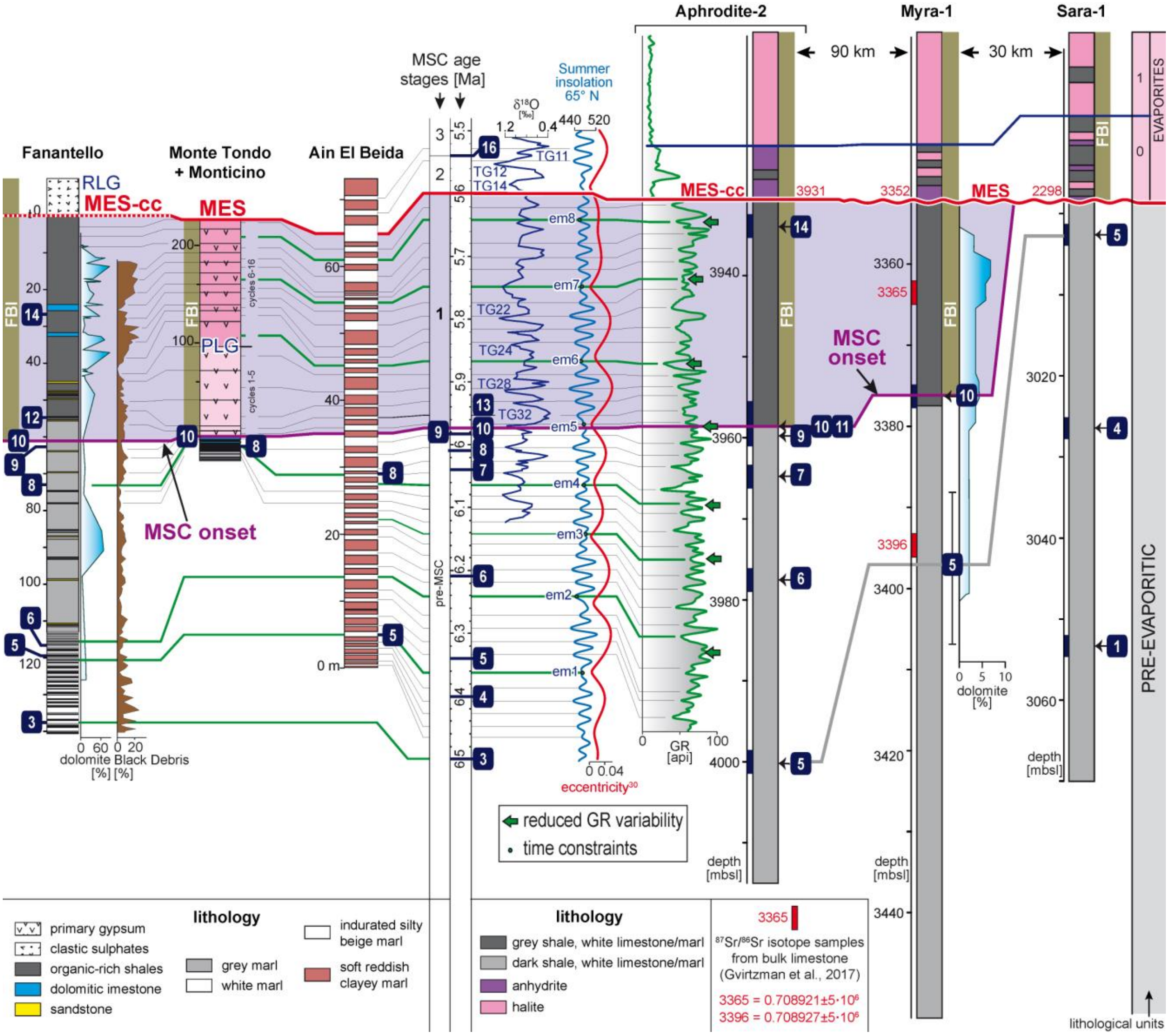
Fanantello
Monte Tondo + Monticino
Ain El Beida
MSC age stages [Ma]
δ18O [‰]
Summer insolation 65° N
eccentricity30
Aphrodite-2
Myra-1
Sara-1
90 km
30 km
RLG
MES-cc
MES
PLG
FBI
MSC onset
pre-MSC
cycles 6-16
cycles 1-5
TG11
TG12
TG14
TG22
TG24
TG28
TG32
em1
em2
em3
em4
em5
em6
em7
em8
dolomite [%]
Black Debris [%]
GR [api]
depth [mbsl]
3931
3352
2298
3365
3396
EVAPORITES
PRE-EVAPORITIC
lithological units
reduced GR variability
time constraints
lithology
primary gypsum
clastic sulphates
organic-rich shales
dolomitic imestone
sandstone
grey marl
white marl
indurated silty beige marl
soft reddish clayey marl
grey shale, white limestone/marl
dark shale, white limestone/marl
anhydrite
halite
87Sr/86Sr isotope samples from bulk limestone (Gvirtzman et al., 2017)
3365 = 0.708921±5·10-6
3396 = 0.708927±5·10-6

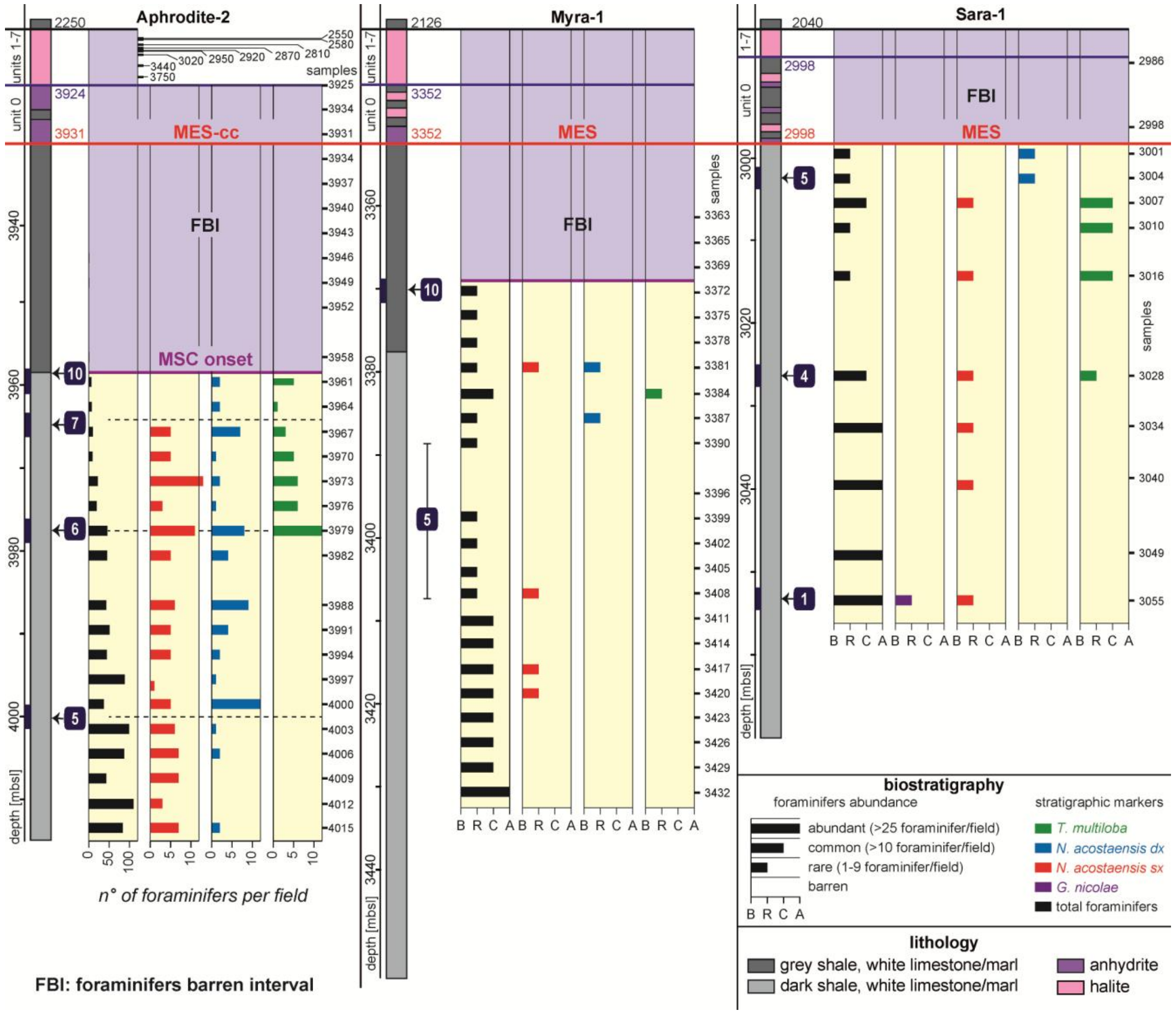
Aphrodite-2
Myra-1
Sara-1
2250
2126
2040
units 1-7
unit 0
3924
3931
3352
2998
samples
MES-cc
MES
FBI
MSC onset
10
7
6
5
4
1
depth [mbsl]
n° of foraminifers per field
0 50 100
0 5 10
B R C A
FBI: foraminifers barren interval
biostratigraphy
foraminifers abundance
abundant (>25 foraminifer/field)
common (>10 foraminifer/field)
rare (1-9 foraminifer/field)
barren
stratigraphic markers
T. multiloba
N. acostaensis dx
N. acostaensis sx
G. nicolae
total foraminifers
lithology
grey shale, white limestone/marl
dark shale, white limestone/marl
anhydrite
halite

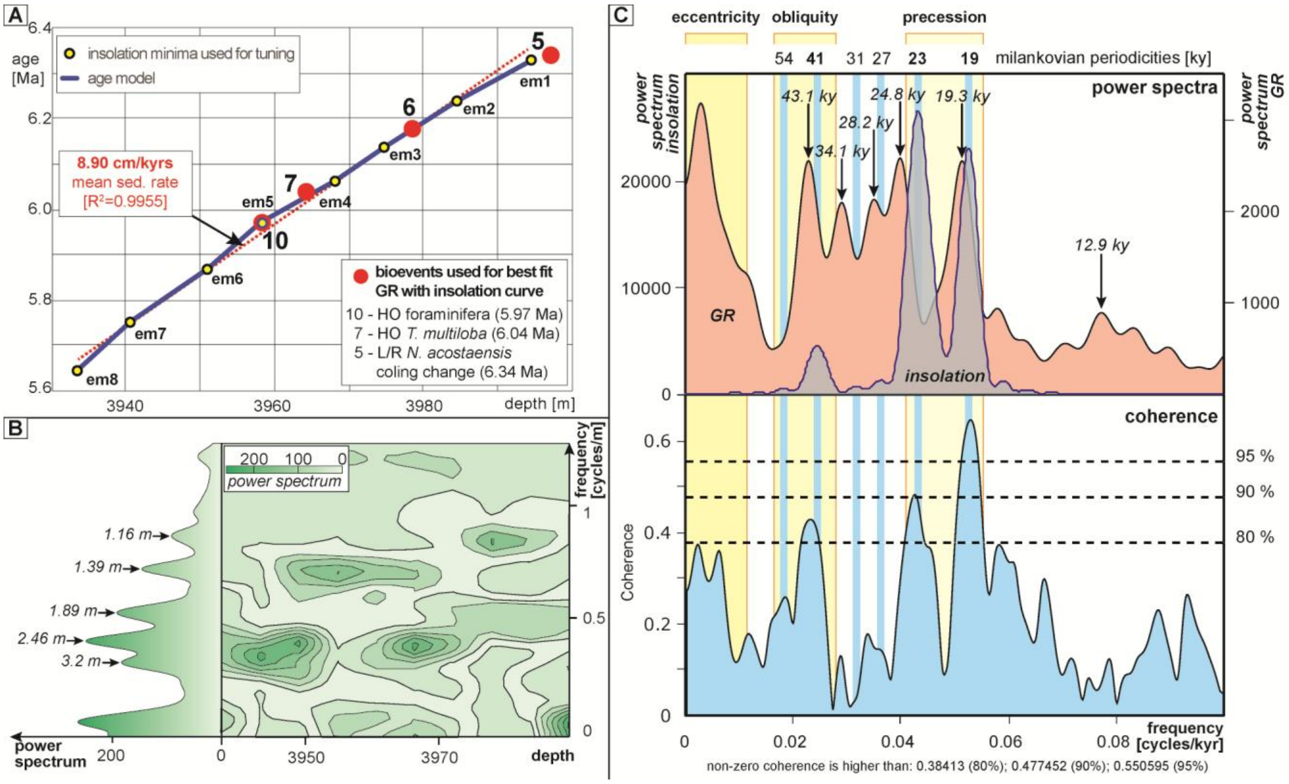
A
age [Ma]
insolation minima used for tuning
age model
8.90 cm/kyrs
mean sed. rate
[R²=0.9955]
em1
em2
em3
em4
em5
em6
em7
em8
5
6
7
10
bioevents used for best fit GR with insolation curve
10 - HO foraminifera (5.97 Ma)
7 - HO T. multiloba (6.04 Ma)
5 - L/R N. acostaensis coling change (6.34 Ma)
6.4
6.2
6.0
5.8
5.6
3940
3960
3980
depth [m]
B
200 100 0
power spectrum
1.16 m
1.39 m
1.89 m
2.46 m
3.2 m
power spectrum
200
0
3950
3970
depth
frequency [cycles/m]
1
0.5
0
C
eccentricity
obliquity
precession
54 41 31 27 23 19 milankovian periodicities [ky]
power spectrum insolation
power spectra
power spectrum GR
43.1 ky
24.8 ky
19.3 ky
28.2 ky
34.1 ky
12.9 ky
GR
insolation
20000
10000
0
2000
1000
coherence
Coherence
95 %
90 %
80 %
0.6
0.4
0.2
0
0
0.02
0.04
0.06
0.08
frequency [cycles/kyr]
non-zero coherence is higher than: 0.38413 (80%); 0.477452 (90%); 0.550595 (95%)

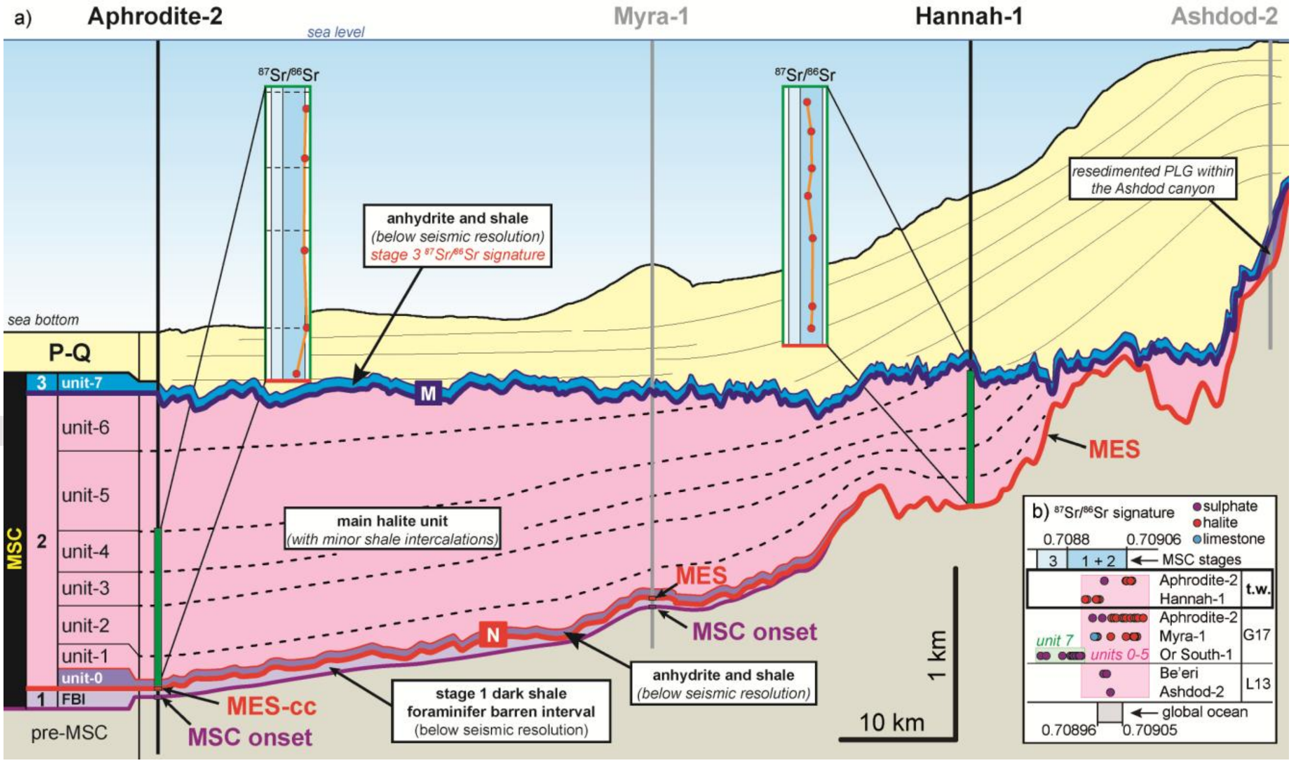
a)
Aphrodite-2
Myra-1
Hannah-1
Ashdod-2
sea level
^{87}Sr/^{86}Sr
^{87}Sr/^{86}Sr
anhydrite and shale
(below seismic resolution)
stage 3 ^{87}Sr/^{86}Sr signature
resedimented PLG within the Ashdod canyon
sea bottom
P-Q
3 unit-7
M
unit-6
unit-5
MSC
2
unit-4
unit-3
unit-2
unit-1
unit-0
1 FBI
pre-MSC
main halite unit
(with minor shale intercalations)
MES
MES
MSC onset
N
anhydrite and shale
(below seismic resolution)
stage 1 dark shale
foraminifer barren interval
(below seismic resolution)
MES-cc
MSC onset
1 km
10 km
b) ^{87}Sr/^{86}Sr signature
sulphate
halite
limestone
0.7088
0.70906
3
1 + 2
MSC stages
Aphrodite-2
Hannah-1
t.w.
Aphrodite-2
Myra-1
Or South-1
G17
unit 7
units 0-5
Be'eri
Ashdod-2
L13
global ocean
0.70896
0.70905

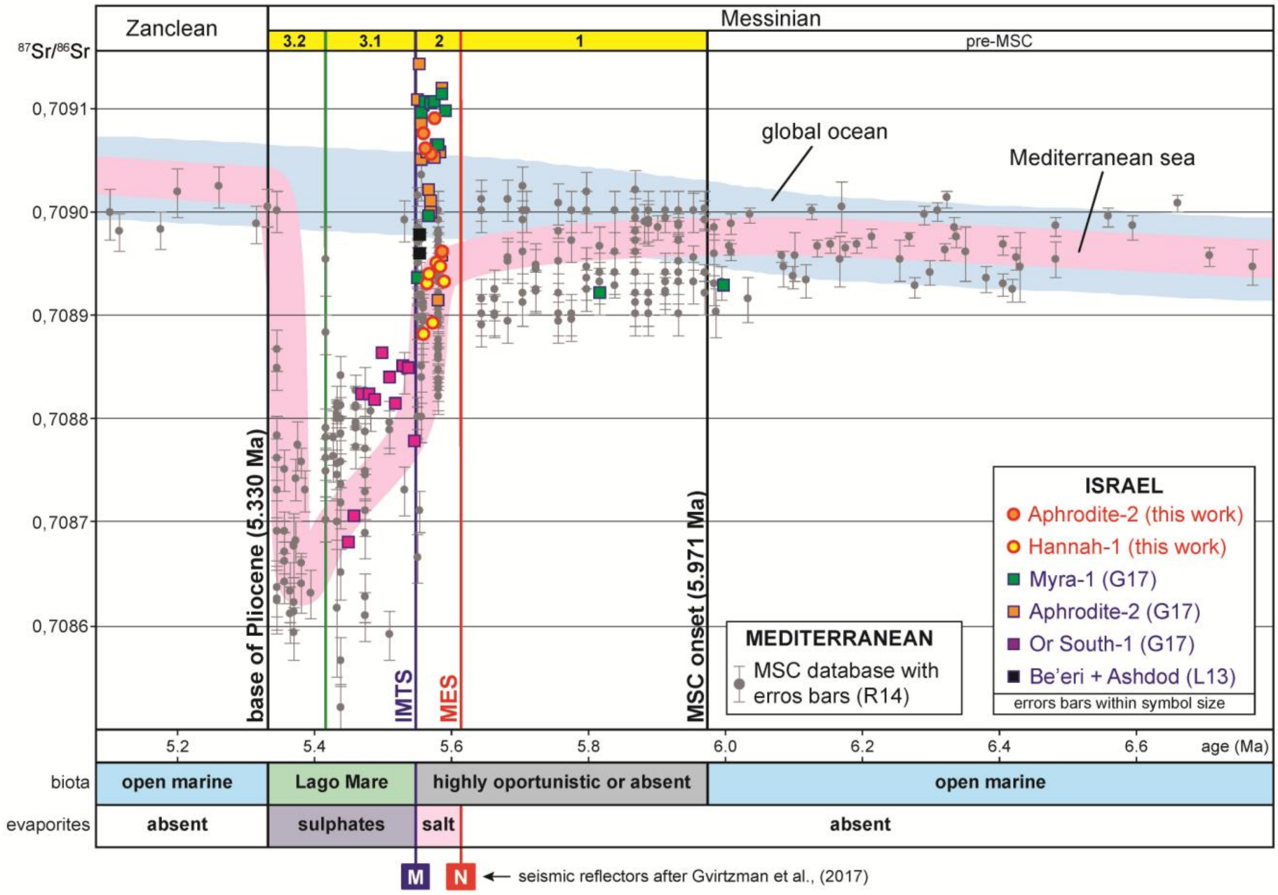
Zanclean
Messinian
3.2
3.1
2
1
pre-MSC
$^{87}Sr/^{86}Sr$
0,7091
0,7090
0,7089
0,7088
0,7087
0,7086
global ocean
Mediterranean sea
base of Pliocene (5.330 Ma)
IMTS
MES
MSC onset (5.971 Ma)
MEDITERRANEAN
MSC database with erros bars (R14)
ISRAEL
Aphrodite-2 (this work)
Hannah-1 (this work)
Myra-1 (G17)
Aphrodite-2 (G17)
Or South-1 (G17)
Be'eri + Ashdod (L13)
errors bars within symbol size
5.2
5.4
5.6
5.8
6.0
6.2
6.4
6.6
age (Ma)
biota
open marine
Lago Mare
highly oportunistic or absent
open marine
evaporites
absent
sulphates
salt
absent
M
N
seismic reflectors after Gvirtzman et al., (2017)